Continuous minimally-invasive alcohol monitoring using microneedle sensor arrays

A.M. Vinu Mohan[a], Joshua Ray Windmiller[b], Rupesh K. Mishra[a], Joseph Wang[a,*]

[a] Department of NanoEngineering, University of California, San Diego, La Jolla, CA 92093, USA
[b] Biolinq inc., 6191 Cornerstone Court East, Suite 109, San Diego, CA 92121, USA

ARTICLE INFO

ABSTRACT

The present work describes an attractive skin-worn microneedle sensing device for the minimally invasive electrochemical monitoring of subcutaneous alcohol. The device consists of an assembly of pyramidal microneedle structures integrated with Pt and Ag wires, each with a microcavity opening. The microneedle aperture was modified by electropolymerizing o-phenylene diamine onto the Pt wire microtransducer, followed by the immobilization of alcohol oxidase (AOx) in an intermediate chitosan layer, along with an outer Nafion layer. The resulting microneedle-based enzyme electrode displays an interference-free ethanol detection in artificial interstitial fluid without compromising its sensitivity, stability and response time. The skin penetration ability and the efficaciousness of the biosensor performance towards subcutaneous alcohol monitoring was substantiated by the ex vivo mice skin model analysis. Our results reveal that the new microneedle sensor holds considerable promise for continuous non-invasive alcohol monitoring in real-life situations.

1. Introduction

Alcoholism represents a major health issue with various health related hazards and potential accident-involved traffic fatalities (Aston and Liguori, 2013; Maenhout et al., 2013; Litten and Allen, 2012; Hawthorne and Wojcik, 2006; Oers et al., 1999). Unhealthy alcohol consumption represents one of the world's leading health risks that results in approximately 2.5 million deaths each year and is a major factor in variety of diseases, disorders and many types of injury. Therefore, there are tremendous needs for easy-to-use accurate alcohol measuring devices that provide reliable and convenient assessment of alcohol consumption and misuse (Dougherty et al., 2014; Swift et al., 1992). Many practical applications would be benefitted from the ability to monitor alcohol continuously in fluids other than blood (Gamella et al., 2014).

Several alcohol monitoring methodologies have been developed, including direct alcohol monitoring from the urine (Jones, 2006), blood (Swift, 2000), saliva (Payne-James et al., 1995), breath (Gullberg, 2003), sweat (Hawthorne and Wojcik, 2006) or interstitial fluid (ISF) (Ridder et al., 2009). Among these, measurements of Blood Alcohol Concentration (BAC) offers accurate alcohol evaluation, but corresponding blood sampling methods (Fingerprick, earlobe) can be painful and inconvenient hence considerably hinder such blood alcohol monitoring route. Breathalyzers (based on Henry's law) are the most commonly used devices for monitoring breath alcohol concentration (BrAC), but to be useful, they require demanding repeated measurements. The performance of BrAC can be affected by local temperature, humidity, environmental fumes (Simpson, 1987; Dumett et al., 2008; Worner and Prabakaran, 1985). Transdermal alcohol sensors (e.g. Giner WrisTAS V) monitor the alcohol content in human perspiration by measuring the current response that corresponds to the alcohol concentration (Dumett et al., 2008). Enzyme-based electrochemical biosensors have been shown recently useful for non-invasive single alcohol measurements in iontophoretically-induced sweat (Kim et al., 2016; Gamella et al., 2014). Alcohol evaluation from ISF of human subjects has indicated a good correlation between ISF and blood alcohol levels (Venugopal et al., 2008). Such evaluation involved extraction of the ISF from micropores (created by a near IR laser) on the stratum corneum layer, by applying vacuum pressure.

Here, we demonstrate a microneedle-based minimally invasive biosensing system for continuous real-time alcohol monitoring from ISF. Microneedles are micron-size low-cost devices capable of physically disrupting the outer layer of the skin to access ISF with negligible damage or pain (Prausnitz, 2004; Kim et al., 2012; Donnelly et al., 2010). Initial efforts have focused on using such microneedle devices for transdermal delivery of drugs and vaccines. Recent activity has led to the development of microneedle diagnostic sensors (P. Miller et al., 2016). These sensing efforts have focused primarily on the minimally-
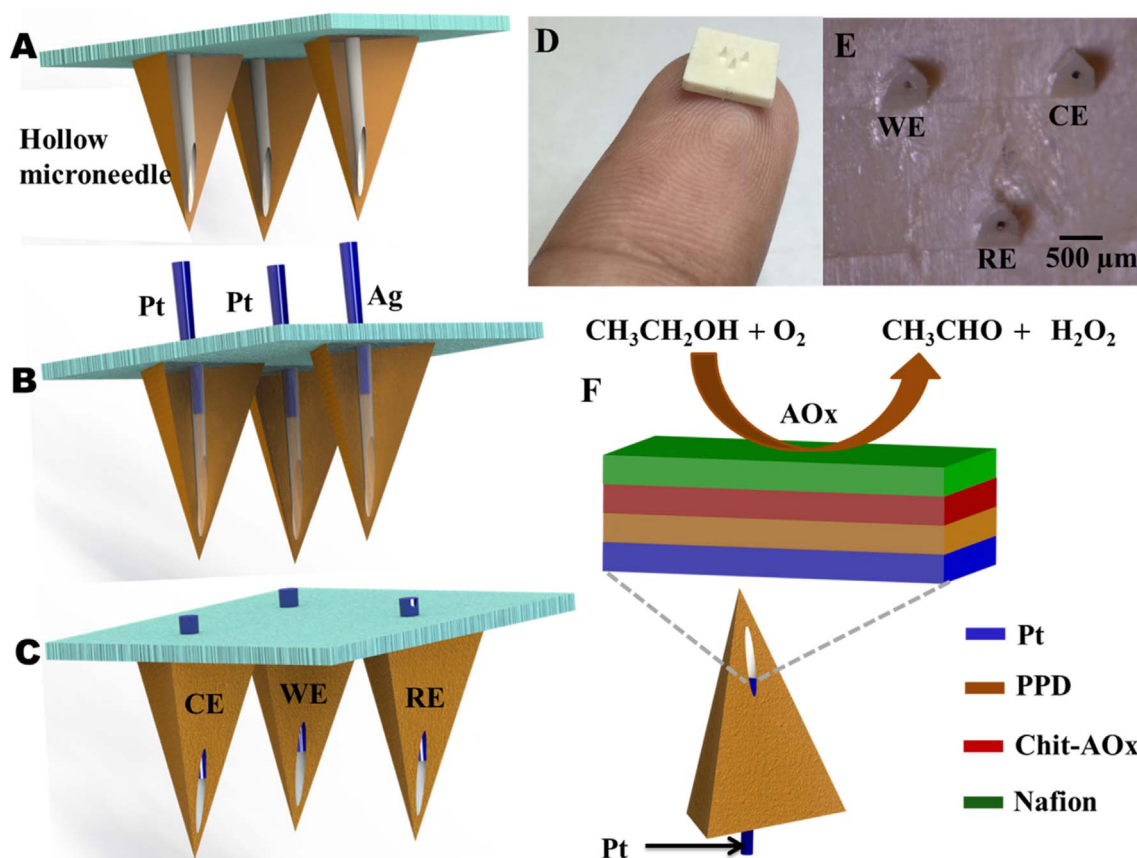
Fig. 1. Schematic representation of a (A) hollow microneedle, (B) press fitting of Pt and Ag wires to the aperture of hollow microneedle and (C) Pt and Ag wires integrated microneedle array. (D) An image showing the microneedle array mounted on the fingertip. (E) Optical micrograph of the microneedle array integrated with Pt and Ag wires. (F) Schematics demonstrating the construction of alcohol biosensor with its multi-layer reagent coating along with the biocatalytic reaction of the immobilized AOx.

invasive electrochemical monitoring of glucose, lactate, glutamate, protein, or potassium (El-Laboudi et al., 2013; Miller et al., 2012; Windmiller et al., 2011a, 2011b; Valdés-Ramírez et al., 2014; Esfandyarpour et al., 2013; Windmiller et al., 2011b; P.R. Miller et al., 2016; Miller et al., 2014).

The present work describes the first example of a microneedle-based minimally invasive biosensor for continuous assessment of alcohol in the ISF (Fig. 1). The microneedle three-electrode system was constructed by integrating Pt and Ag wires within the aperture of hollow microneedles (Fig. 1A). Functionalizing the Pt-wire working-electrode transducer with the AOx enzyme, along with a perm-selective reagent layer, imparted high selectivity and stability towards the ethanol substrate and enabled the continuous monitoring of alcohol from artificial ISF. The ability of the microneedle system to penetrate the skin and measure alcohol level from the ISF was validated ex vivo using a mice skin model. The attractive analytical performance of the new microneedle sensor makes it extremely attractive as a minimally-invasive wearable transdermal device for continuous subcutaneous monitoring of alcohol.

2. Materials and methods

2.1. Reagents and instrumentation

Alcohol oxidase from Pichia pastoris (10–40 units/mg protein), o-Phenylenediamine (o-PD), potassium phosphate monobasic (KH_2PO_4), and potassium phosphate dibasic (K_2HPO_4), sodium chloride, potassium chloride, D-(+)- Glucose, sucrose, sodium gluconate, chitosan, Nafion®, acetaminophen, ascorbic acid, uric acid, bovine serum albumin, calcium chloride anhydrous and magnesium sulfate anhydrous were purchased from Sigma-Aldrich and ethyl alcohol was obtained

from Decon Labs. Electrochemical measurements were conducted using a CH Instrument potentiostat (model 1232, Austin, TX, USA) connected to a PC, was employed for the electrochemical studies. Optical images were recorded by an optical microscope (Motic SMZ-168 Series) coupled with a digital camera (Nikon, D7000).

2.2. Fabrication of microneedle array

Cost-effective, scalable micro-injection molding techniques for the high-volume manufacture of robust microneedle transducers have been developed for continuous assessment of circulating analytes in the ISF. A press-fitting process has been implemented whereby 100 μm-diameter platinum and silver wires are inserted into selected sites in the microneedle lumen in order to construct the electrochemical transducer, which is accessible for functionalization via the hollow microneedle aperture (Fig. 1).

In order to realize the construction of microneedles possessing suitable mechanical properties (stiffness, tensile strength, resistance to plastic deformation), a medical-grade liquid crystal polymer (LCP) is utilized in the injection-molding process (biocompatible per ISO10993 or USP Class VI). The blend used in the injection molding process has been selected for its outstanding mechanical properties -a tensile modulus of 2350 MPa, a flexural modulus of 2300 MPa, and a hardness of 118 on the Rockwell scale. Three-dimensional renderings of the three-element hollow microneedle array were designed in AutoCAD and implemented in a high-carbon stainless steel mold that was etched using a precision computer numerical control (CNC) mill. Design criteria included positioning the hollow aperture (creating an accessible lumen for the electrochemical transducer) in as close proximity to the microneedle tip as possible without compromising the structural resiliency of the microneedle structure due to decreased wall thickness.

Furthermore, the mold process was optimized to minimize tip radius to maximize the penetration / insertion force exerted by each microneedle constituent to permeate the stratum corneum and access the ISF.

Upon construction, the microneedle arrays were evaluated using a computer-controlled precision force-displacement tester to quantify insertion forces and understand the interplay between microneedle geometry, skin penetration, and force applied. A biological stain (methylene blue) was subsequently utilized to confirm permeation of the stratum corneum (porcine skin), as evaluated using optical microscopy. Highly sensitive measurements of electrical conductivity were also performed upon insertion of the microneedle array into the skin sample and permeation of the stratum corneum to access the ISF was corroborated by a marked increase in measured current at a fixed applied potential. Following several design iterations, it was determined that microneedles possessing a height of 800 μm, edge width between 320 and 460 μm, 116.6° sidewall slope, and circular aperture of diameter 100 μm, centered approximately at 520 μm distal to the substrate were best able to penetrate the stratum corneum to access the viable interstitial fluid.

2.3. Biosensor construction

The microcavity present in the microneedle array lends to create a stable enzyme layer without affecting its skin penetration capability. Initially, in order to reject the potential electroactive interferents, poly(*o*-phenylenediamine) (PPD) film was electropolymerized from a solution of o-PD on the Pt wire integrated microneedle (working) electrode. The electropolymerization was performed by applying a constant electrode potential of 0.65 V for 15 min in a deaerated 50 mM o-PD prepared in acetate buffer (pH 4.5). The alcohol oxidase (AOx) enzyme was further immobilized on PPD film modified Pt-microneedle using chitosan as a binder. Initially, the buffered aqueous solution of AOx containing ~25 units/mg protein was mixed with chitosan (2% w/v) prepared in 1 M acetic acid (1:1 ratio). Subsequently, 3 μL of the mixture was casted over the PPD modified Pt electrode and allowed to dry under ambient conditions. The enzyme modified microneedles were further modified with 1 μL of Nafion (1%, w/v) prepared in ethanol. The biosensor array was kept at 4 °C overnight. A schematic illustration of this protocol is shown in Fig. 1F.

2.4. In vitro evaluation

The electrochemical performance of the microneedle biosensor array was evaluated in vitro using 0.1 M phosphate buffer (pH 7.0) solution. Chronoamperometric responses were recorded at 0.6 V (vs. Ag/AgCl reference electrode) after 100 s incubation in the sample solution. The artificial ISF was prepared by following the reported procedure (Bretag, 1969). The effect of electroactive interferents, such as uric acid (UA), acetaminophen (AC) and ascorbic acid (AA) towards the alcohol biosensor was analyzed. The operational stability of the alcohol biosensor was examined by performing repetitive chronoamperometric measurements. Ultra-pure deionized water (18.2 MΩ cm) was used to prepare all solutions.

2.5. Ex vivo skin model evaluation

The performance of the microneedle biosensor array was assessed ex vivo by using a mice skin model towards detecting ethanol in the interstitial fluid. The mice skin samples were collected and stored at −20 °C prior to use. The samples were thawed at room temperature and cut in to small pieces. The microneedle biosensor array was manually penetrated through the skin sample. The ex vivo alcohol detection study was performed in a compartment filled with artificial ISF containing 20.1 mg/mL BSA. The microneedle array, penetrated the skin sample, was carefully placed over the compartment and was allowed to dip the penetrated microneedle tips into the solution. The chronoamperometric response was measured at 0.6 V (vs. Ag/AgCl electrode) after 100 s incubation in the sample solution.

3. Results and discussion

3.1. Design and optimization

The new minimally-invasive alcohol biosensor system was constructed by using an array of sharp hollow microneedles having a microcavity to access the ISF (Fig. 1A). Pt and Ag wires (100 μm diameter) were inserted into the hollow aperture (Fig. 1B) to create the working, counter and reference electrodes, respectively (Fig. 1C). Optical images of the resulting 3-electrode microneedle array are displayed in Fig. 1D. The close-up image of Fig. 1E depicts the nonplanar feature of the pyramidal microneedle array with triangular bases (1.5 mm separation; 800 μm height) as well as the cylindrical openings (100 μm diameter). The working-electrode transducer was functionalized initially by electropolymerization of a size-exclusion PPD layer over the Pt wire integrated microneedle, followed by immobilization of the AOx enzyme within a chitosan matrix and subsequent coverage with a Nafion film (Fig. 1F).

The hydrogen peroxide (H_2O_2), generated by the AOx catalyzed oxidation of ethanol, is selectively transported through the size-exclusion PPD film and detected at Pt electrode transducer; the oxidation current of the peroxide enzymatic product thus correlates to the target ethanol concentration. The chitosan layer provides a stable and biocompatible environment for the enzyme molecules while the outer Nafion layer prevents leaching of the biosensor constituents and excludes the negatively-charged interferents. The analytical performance of the alcohol biosensor was characterized first in-vitro using phosphate buffer (pH 7) as well as in artificial ISF containing 20.1 mg/mL BSA.

Initial electrochemical studies were conducted to characterize the response of unmodified Pt wire integrated microneedle electrode towards H_2O_2 (the detectable byproduct of the AOx reaction). The chronoamperometric response for 250 μM H_2O_2 (in phosphate buffer) was measured at different potentials, ranging from −0.2 to 0.6 V (Fig. 2A). The H_2O_2 reduction current increases rapidly upon raising the potential between −0.05 V and −0.20 V. In contrast, the H_2O_2 oxidation current increases slowly upon changing the potential between −0.05 V and +0.60 V. Such profile reflects the catalytic activity of the Pt wire transducer. Such hydrodynamic voltammogram is in agreement with corresponding cyclic voltammograms (CV) for 500 μM H_2O_2 (shown as an inset). A similar CV profile for H_2O_2 was obtained also in artificial ISF (not shown), indicating that the different media compositions have negligible effect upon the redox behavior of H_2O_2. Subsequent amperometric work employed an operating potential of +0.60 V that offers the most favorable sensitivity.

The sensitivity of the unmodified microneedle array electrode towards H_2O_2 was evaluated over the 50−400 μM range. As illustrated in Fig. 2B, the Pt wire integrated microneedle sensor displays a linear response to H_2O_2 using an operating potential of 0.6 V. The corresponding calibration plot has a sensitivity of 0.0057 nA/μM (with a correlation coefficient, R^2 =0.9957; Relative Standard Deviation, RSD =1.8%, n=4).

3.2. Biosensor performance

The analytical response of the microneedle biosensor towards alcohol was evaluated by recording chronoamperometric responses in phosphate buffer having 0 mM to 80 mM ethanol. The current was sampled for 35 s at an applied working potential of 0.6 V vs. Ag/AgCl reference electrode. Fig. 3A displays chronoamperograms for increasing alcohol concentrations (0−80 mM, a-q), along with the corresponding calibration plot (inset). Well defined signals are observed over the entire range. The current increases linearly with the concentration,
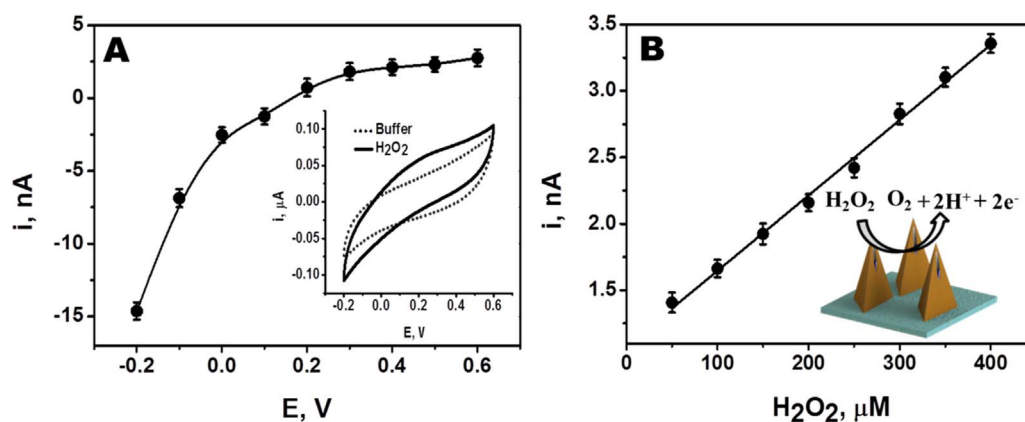
Fig. 2. (A) Effect of applied potential (−0.2–0.6 V) on the chronoamperometric responses of 250 μM H_2O_2 measured at Pt wire integrated microneedle electrode. Also shown (inset) the corresponding cyclic voltammogram for 500 μM H_2O_2. (B) Linear chronoamperometric responses of H_2O_2 (50–400 μM) measured at Pt wire integrated microneedle electrode (inset shows the oxidation of H_2O_2 on the Pt wire integrated microneedle electrode).

with a sensitivity of 0.062 nA/mM and correlation coefficient of 0.9886 (RSD =3.3%, n=5). These results showed that the biosensor possesses a wide range of detection with appreciable sensitivity.

The biosensor response was also studied in artificial interstitial fluid. Fig. 3B demonstrates chronoamperograms for 16 successive 5 mM increments in the ethanol concentration (*a*-q). Well defined current signals, proportional to the ethanol concentration, are observed over the entire 0–80 mM range. The resulting calibration plot (shown in the inset) is linear with a sensitivity of 0.0452 nA/mM and correlation coefficient of 0.9930 (RSD =3.56%, n =5). Such response in artificial ISF indicates the potential for subcutaneous alcohol monitoring, as supported by the mice-skin ex-vivo experiments (described below).

Since the microneedle biosensor is aimed to detect alcohol from human interstitial fluid, the device should offer high selectivity in presence of common physiological electroactive constituents, such as UA, AC and AA, that can cause interference with the amperometric response of alcohol. Accordingly, the new biosensor was designed to minimize potential electroactive interferences by combining two perm-selective layers: a size-exclusion PPD film and charged-exclusion Nafion (Dempsey et al., 1993; Lowry et al., 1994). The latter can effectively exclude negatively-charged electroactive interferents from the electrode surface. The selectivity of the biosensor was evaluated by measuring the chronoamperometric alcohol response in the presence and absence of the common interferents at relevant physiological concentrations (Trengove et al., 1996). Fig. 4 displays the current response for 20 mM ethanol in the absence and presence of 100 μM of AC, UA and L-cysteine and 10 μM AA. The percentage deviation of the
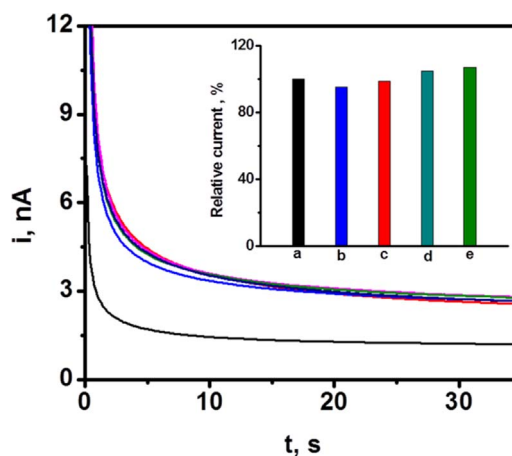

Fig. 4. Chronoamperometric response of the alcohol biosensor for 20 mM alcohol followed by the addition of electroactive interferents such as AC, UA, L-Cysteine and AA, respectively (0.6 V vs. Ag/AgCl electrode). Inset shows the percentage deviation of relative current responses based on (a) 20 mM alcohol signal for 100 μM each of (b) AC, (c) UA and (d) L-Cysteine and 10 μM AA, respectively. The blank response is also shown (black curve). Conditions, as in Fig. 3.

sensor response in the presence of these potential interferents is also presented (inset, Fig. 4). These co-existing compounds have a minimal effect upon the alcohol response, with up to 6% variation in the signal. Apparently, the PPD/Nafion multi-layer surface coating of the micro-needle Pt transducer serves as an effective anti-interference barrier.
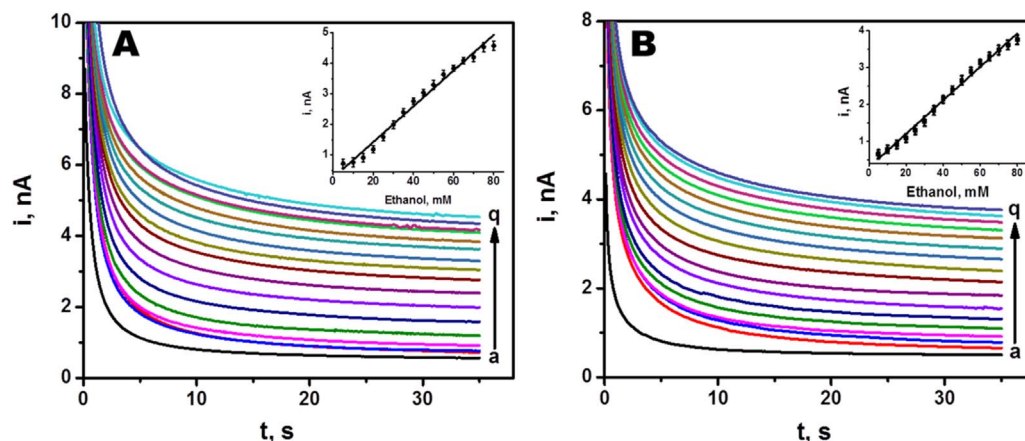

Fig. 3. Chronoamperometric responses of the alcohol biosensor recorded in (A) phosphate buffer of pH 7 and (B) in artificial ISF from 0 to 80 mM alcohol in 5 mM increments (from a-q) at 0.6 V vs. Ag/AgCl electrode. (Inset shows the corresponding calibration plots. Current Sampling interval: 0.1 s over 35 s. Other conditions, as in Fig. 2.
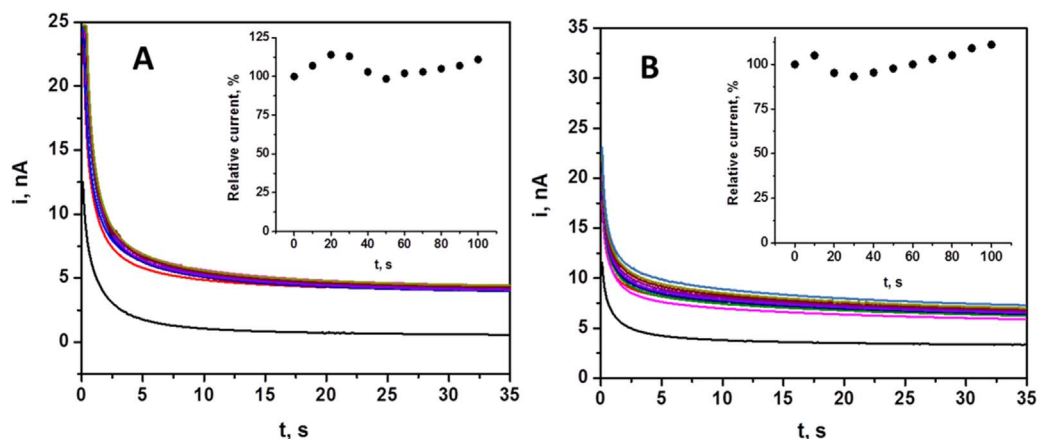
Fig. 5. Operational stability of the microneedle alcohol biosensor. Response to 30 mM alcohol in (A) phosphate buffer and (B) artificial ISF containing 20.1 mg/mL BSA over 100 min periods at 10 min intervals. Conditions, as in Fig. 3.

3.3. Continuous monitoring of alcohol

The long term operational stability of the biosensor is a prerequisite factor in terms of real time alcohol monitoring from the body. The stability of the microneedle based alcohol biosensor was examined by measuring chronoamperometric responses of 30 mM alcohol at regular intervals for 100 min Fig. 5A illustrates that this experiment resulted in highly reproducible alcohol signals. The inset shows the relation between percentage deviations of current responses with respect to time, indicating small variations in the sensor response throughout this series of repetitive measurements (RSD =1.52%, n=4).

The continuous exposure of subcutaneous electrochemical sensors to complex medium may affect their sensor response due to potential fouling by coexisting protein molecules. Hence, it is essential to evaluate the performance of the new microneedle alcohol biosensor in artificial interstitial fluid. The operational stability of the alcohol biosensor was thus investigated in complex artificial ISF containing 20.1 mg/mL BSA. Fig. 5B shows the amperometric response (30 mM) recorded over a 100 min period at regular intervals of 10 min. The inset reveals the relation between percentage deviations of current responses with respect to time. These data indicate less than 10% variation compared to the initial alcohol response, supporting potential applications of the developed alcohol biosensor (RSD =2.85%).

3.4. Ex vivo skin model evaluation

The efficacy of the microneedle array based alcohol biosensor for the subcutaneous alcohol measurements was explored ex vivo by using the mice skin model, as demonstrated in Fig. 6A. The microneedle sensor was carefully penetrated through the mice skin sample, placed over the artificial ISF compartment in such a way to dip the microneedle tips into the solution. The alcohol concentration in the ISF compartment was increased linearly and the corresponding chronoamperometric signals were recorded at 0.6 V. Well defined response is thus observed for increasing the ethanol concentration in 25 µM steps. These data and the corresponding linear calibration plot corroborate that the microneedle biosensor can be readily integrated on the skin and it detect alcohol from the interstitial fluid. The microneedle tips are found to be quite sharp (Fig. 6C) to allow convenient penetration into thin mice skin specimen (Fig. 6D) by applying a gentle pressure on it. The microneedle array was observed to maintain its morphology and mechanical properties even after multiple skin penetrations (Fig. 6E). Also, the ex vivo skin model evaluation showed that the skin worn sensor exhibits similar sensitivity to that observed during in vitro studies (Fig. 3B). Overall, this experiment indicates that the microneedle alcohol biosensor possesses a stable enzymatic layer which is unaffected by the skin penetration process. Apparently, the microcavity
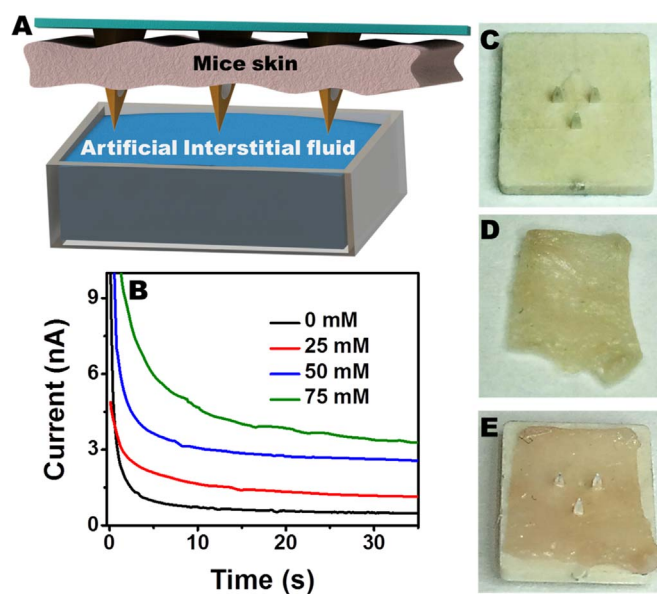

Fig. 6. (A) Schematic showing the detection of alcohol in artificial ISF using the microneedle penetrated through the mice skin. (B) Real-time alcohol detection from the artificial ISF using the microneedle penetrated through the mice skin. A close up image showing the (C) microneedle biosensor array, (D) mice skin sample and (E) the penetrated microneedle through the mice skin. Other conditions, as in Fig. 3.

within the microneedle helps to protect the immobilized enzyme layer during the skin penetration and allows to access the viable ISF.

4. Conclusions

The present study has demonstrated the design and performance of a microneedle-based enzymatic (AOx) electrochemical sensor for minimally-invasive continuous monitoring of alcohol. Such development addresses the urgent demands for continuous alcohol-monitoring devices. The new biosensor device incorporates Pt and Ag wires within the hollow microneedle aperture and the presence of microcavity protects the enzyme layer upon skin penetration. A multilayer PPD/Nafion coating serves as an effective permselective/protective barrier, excluding potential interferents away from the transducer surface. The biosensor array displays an attractive analytical performance with high selectivity and stability that make it appropriate platform for continuous monitoring of alcohol. The ex vivo mice skin model analysis substantiated the performance of the microneedle array towards subcutaneous alcohol ISF detection. Future efforts are aimed at integrating the corresponding electronic backbone for powering the

sensor, along with signal processing and wireless communication on the microneedle platform, and evaluating and validating the integrated wearable transdermal device in a large-scale alcohol monitoring study. Such developments should lead to a wireless minimally-invasive alcohol detection system that will enable real-time remote monitoring of individuals while eliminating blood sampling complications.

Acknowledgement

References

Aston, E.R., Liguori, A., 2013. Addict. Behav. 38, 1944–1951.

Bretag, A.H., 1969. Life Sci. 8, 319–329.

Dempsey, E., Wang, J., Smyth, M.R., 1993. Talanta 40, 445–451.

Donnelly, R.F., Singh, T.R.R., Woolfson, A.D., 2010. Drug. Deliv. 17, 187–207.

Dougherty, D.M., Hill-Kapturczak, N., Liang, Y., Karns, T.E., Cates, S.E., Lake, S.L., Mullen, J.J., Roache, D., 2014. Drug Alcohol Depend. 142, 301–306.

Dumett, M.A., Rosen, I.G., Sabat, J., Shaman, A., Tempelman, L., Wang, C., Swift, R.M., 2008. Appl. Math. Comput. 196, 724–743.

El-Laboudi, A., Oliver, N.S., Cass, A., Johnston, D., 2013. Diabetes Technol. Ther. 15, 101–115.

Esfandyarpour, R., Esfandyarpour, H., Javanmard, M., Harris, J.S., Davis, R.W., 2013. Sens. Actuat. B-Chem. 177, 848–855.

Gamella, M., Campuzano, S., Manso, J., de Rivera, G.G., López-Colino, F., Reviejo, A.J., Pingarrón, J.M., 2014. Anal. Chim. Acta 806, 1–7.

Gullberg, R.G., 2003. Forensic Sci. Int. 131, 30–35.

Hawthorne, J.S., Wojcik, M.H., 2006. Can. Soc. Forensic Sci. J. 39, 65–71.

Jones, A.W., 2006. Toxicol. Rev. 25, 15–36.

Kim, J., Jeerapan, I., Imani, S., Cho, T.N., Bandodkar, A., Cinti, S., Mercier, P.P., Wang, J., 2016. ACS Sens 1, 1011–1019.

Kim, Y.C., Park, J.H., Prausnitz, M.R., 2012. Adv. Drug. Del. Rev. 64, 1547–1568.

Litten, R.Z., Allen, J.P., 2012. Springer Sci. Bus. Media, (New York).

Lowry, J.P., McAteer, K., El Atrash, S.S., Duff, A., O'Nelll', R.D., 1994. Anal. Chem. 66, 1754–1761.

Maenhout, T.M., De Buyzere, M.L., Delanghe, J.R., 2013. Clin. Chim. Acta 415, 322–329.

Miller, P., Moorman, M., Manginell, R., Ashlee, C., Brener, I., Wheeler, D., Narayan, R., Polsky, R., 2016. Electroanalysis 28, 1305–1310.

Miller, P.R., Narayan, R.J., Polsky, R., 2016. J. Mater. Chem. B. 4, 1379–1383.

Miller, P.R., Skoog, S.A., Edwards, T.L., Lopez, D.M., Wheeler, D.R., Arango, D.C., Xiao, X., Brozik, S.M., Wang, J., Polsky, R., Narayan, R.J., 2012. Talanta 88, 739–742.

Miller, P.R., Xiao, X., Brener, I., Burckel, D.B., Narayan, R., Polsky, R., 2014. Adv. Healthc. Mater. 3, 876–881.

Oers, J.A.M.V., Bongers, I.M.B., Van de Goor, L.A.M., Garretsen, H.F.L., 1999. Alcohol Alcohol. 34, 78–88.

Payne-James, J.J., Keys, D.W., Jerreat, P.G., 1995. J. Clin. Forensic Med. 2, 41–44.

Prausnitz, M.R., 2004. Adv. Drug Deliv. Rev. 56, 581–587.

Ridder, T.D., Steeg, B.J.V., Vanslyke, S.J., Way, J.F., 2009. Optical Diagnostics and Sensing IX, Proceedings of SPIE, 7186.

Simpson, G., 1987. Clin. Chem. 33, 261–268.

Swift, R., 2000. Alcohol Clin. Exp. Res. 24, 422–423.

Swift, R.M., Martin, C.S., Swette, L., LaConti, A., Kackley, N., 1992. Alcohol Clin. Exp. Res. 16, 721–725.

Trengove, N.J., Langton, S.R., Stacey, M.C., 1996. Wound Repair Regen. 4, 234–239.

Valdés-Ramírez, G., Li, Y., Kim, J., Jia, W., Bandodkar, A.J., Nuñez-Flores, R., Miller, P.R., Wu, S., Narayan, R., Windmiller, J.R., Polsky, R., Wang, J., 2014. Electrochem. Commun. 47, 58–62.

Venugopal, M., Feuvrel, K.E., Mongin, D., Bambot, S., Faupel, M., Panangadan, A., Talukder, A., Pidva, R., 2008. IEEE Sens. J. 8, 71–80.

Windmiller, J.R., Valds-Ramrez, G., Zhou, N., Zhou, M., Miller, P.R., Jin, C.S., Brozik, M., Polsky, R., Katz, E., Narayan, R., Wang, J., 2011a. Electroanalysis 23, 2302–2309.

Windmiller, J.R., Zhou, N., Chuang, M., Valdes-Ramírez, G., Santhosh, P., Miller, P.R., Narayan, R., Wang, J., 2011b. Analyst 136, 1846–1851.

Worner, T.M., Prabakaran, J., 1985. Alcohol 20, 349–350.